We are IntechOpen, the world's leading publisher of Open Access books Built by scientists, for scientists

4,800
Open access books available

122,000
International authors and editors

135M
Downloads

Our authors are among the

154
Countries delivered to

TOP 1%
most cited scientists

12.2%
Contributors from top 500 universities

CLARIVATE ANALYTICS BOOK CITATION INDEX INDEXED

WEB OF SCIENCE™

Selection of our books indexed in the Book Citation Index in Web of Science™ Core Collection (BKCI)

Interested in publishing with us?
Contact book.department@intechopen.com

Numbers displayed above are based on latest data collected.
For more information visit www.intechopen.com

Chapter 8

Self-Calibration of Two-Dimensional Precision Metrology Systems

Chuxiong Hu and Yu Zhu

Additional information is available at the end of the chapter

http://dx.doi.org/10.5772/62761

Abstract

In modern industry, there usually exist high-precision stages, such as reticle stages and wafer stages in VLSI lithography tools, metrology stages in coordinate measurement machines, motion stages in CNC machine tools, etc. These stages need high-precision measurement/metrology systems for monitoring its XY movement. As the metrology systems are quite accurate, we often cannot find a standard tool with better accuracy to implement a traditional calibration process for systematic measurement error (i.e., stage error) determination and measurement accuracy compensation. Subsequently, self-calibration technology is developed to meet this challenge and to solve the calibration problem. In this chapter, we study the self-calibration of two-dimensional precision metrology systems and present a holistic self-calibration strategy. This strategy utilizes three measurement views of an artifact plate with mark positions not precisely known on the un-calibrated two-dimensional metrology stage and constructs relevant symmetry, transitivity, and redundancy of the stage error of the metrology stage. The misalignment errors of all measurement views, especially including those of the translation view, are totally determined by detailed mathematical manipulations. Then, a redundant equation group is synthesized, and a least-square–based robust estimation law is employed to calculate out the stage error even under the existence of random measurement noise. Furthermore, as the determination of the misalignment error components of the measurement views is rather complicated but important in previous and the proposed methods, this chapter also significantly analyzes the necessity of this costly computation. The proposed approach is investigated by simulation computation, and the simulation results prove that the proposed determination scheme can calculate out the stage error rather exactly without random measurement noise. Furthermore, when there exist various random measurement noises, the calibration accuracy of the proposed strategy is also investigated, and the results illustrate that the standard deviations of the calibration error are consistently with the same level of those of the random measurement noises. All these results verify that the proposed scheme can realize the stage error rather accurately even under the existence of random measurement noise. The practical

procedure for performing a standard self-calibration is also introduced for engineers to facilitate actual implementation.

Keywords: Self-calibration, Metrology system, Stage error, Measurement noise, VLSI lithography

1. Introduction

Modern precision applications such as VLSI lithography tools, CNC machine tools, and coordinate measurement machines usually need multi-dimensional stages those are capable of manufacture accuracy at micro/nanometer levels [1, 2]. As automatic servo systems, these stages have metrology/measurement systems for position information and motion feedback [3–5]. Because of the unavoidable surface non-flatness, non-orthogonality, scale difference, etc., in the metrology systems, there exists systematic measurement error (i.e., stage error), which is the difference between the actual metrology system and the ideal metrology system [6]. The common way to determine the stage error map in Cartesian space needs traditional calibration technology [7, 8] with a rather standard measurement plate or scale for direct "high-precision calibrates low-precision". If the stage error can be figured out, the measurement accuracy of the metrology system in the stage could be determined and compensated, which will improve the positioning accuracy and repeatability of practical motion systems [9, 10]. However, in practical ultra-precision applications such as nano-lithography, engineers usually cannot find a standard measurement tool with better accuracy than the stage's metrology system to perform a traditional calibration process. Therefore, the idea of self-calibration is developed. The basic principle is to utilize an artifact plate with mark positions not precisely known and place the plate on the metrology stage with different locations or orientations to construct different measurement views [11]. In the following **Figure 1**, one example of the measurement view is shown where the pedestal is the un-calibrated metrology system and the grid plate is the artifact plate.

The key point of the self-calibration way is that the positions of the marks on the plate are fixed whatever the measurement view is, and researchers could utilize the measurement information of the marks in different views to construct equation about the stage error for final determination. Following this way, self-calibration has attracted attention of researchers and engineers and has been applied to certain special but important applications [12, 13], such as nano-positioners [14], profiling stages [15], scanning probe microscope [16], and coordinate measuring machines [17]. For example, Takac [18] concerned the self-calibration problem of one-dimensional stages with the utilization of an un-calibrated artifact plate to obtain congruency via transitivity and provided a calibration that makes a set of tool graduation markers with identical spacing. Raugh proposed a rigorous mathematical method for two-dimensional self-calibration under the assumption that the stage error map in Cartesian space can be expressed as a finite polynomial [19]. However, the scheme is complicated with extensive computation and even may be unstable under the existence of random measurement noise. To reduce the computation of Raugh's algorithm, for the two-dimensional self-calibration, Takac et al. [9] developed a transitive algorithm based on direct point-to-point comparison,

http://dx.doi.org/10.5772/62761

which is intuitive and simple, but quite sensitive to random measurement noise due to that the handling of the rotation and translation of each measurement view is oversimplified.

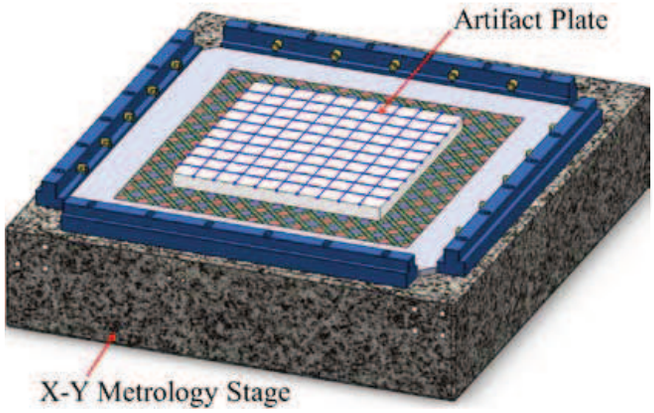

Figure 1. An artifact plate on a two-dimensional metrology stage.

In [20], Ye proposed a discrete Fourier transform-based algorithm for two-dimensional self-calibration, which is numerically robust. He also validated that the algorithm provides an exact self-calibration on the discrete sample sites when there was no random measurement noise, and only introduced calibration error of about the same size as the random measurement noise when there exists random measurement noise. The development of this algorithm is inspired by the achievement of Takac and Raugh and is considered as a standardized process by related researchers and engineers [16]. However, the computation for the misalignment error components of translation view is complex due to that the information of the rotation view is not sufficiently utilized. Moreover, discrete Fourier transform is widely used in the algorithm, which further increases the difficulty on understanding and implementation for researchers and engineers [21].

In this chapter, considering the complexity of existing algorithms, the self-calibration of X–Y precision metrology stages is studied with simplicity and effectiveness orientation. The method sufficiently utilizes the three properties of stage error detailed in [20] but abandons the Fourier transform way to provide an easily understood self-calibration algorithm. Specifically, with the three measurement views of the plate on the un-calibrated stage, the measurement information of the plate's mark positions in all views is utilized to construct symmetry, transitivity, and redundancy of the stage error. Consequently, a least-square-based self-calibration algorithm is proposed to effectively realize the stage error accurately even under the existence of random measurement noise. The computation process for the components of misalignment error of each measurement view is also provided in detail, which could be utilized as basis for synthesis of other self-calibration strategies. Furthermore, as the determination of the misalignment error components of the measurement views is rather complicated but important in previous and the proposed methods, this chapter also significantly analyzes the necessity of this costly computation. The proposed self-calibration algorithm is investigated by computer simulation, and the results validate that the stage error could be determined quite exactly when there is no random measurement noise. Furthermore, when there exists

random measurement noise, the calibration accuracy also could be guaranteed, and the calibration error is at the same level as the random measurement noises, which illustrates that the proposed scheme possesses certain performance robustness. The proposed scheme actually develops a well-understood solution to two-dimensional self-calibration problem, which could facilitate practical implementation.

2. Problem formulation of two-dimensional self-calibration

2.1. Stage error

In this section, the expression of stage error would be presented. In a two-dimensional metrology/measurement system of the stage, define (x, y) as the true location of the sample site in the Cartesian grid, and **G**(x, y) as the stage error at (x, y), which is the difference between the actual metrology/measurement system and the ideal metrology/measurement system. The field to be calibrated is assumed to be L × L, and the origin of the X–Y axis is at the center of this area. Define

$$\mathbf{G}(x,y) = G_x(x,y)\mathbf{e}_x + G_y(x,y)\mathbf{e}_y \tag{1}$$

where $\mathbf{e}_x$ and $\mathbf{e}_y$ are the unit vectors of the two-dimensional stage axis; $G_x(x, y)$ and $G_y(x, y)$ are functions of the continuous X–Y field L × L. The sample sites are set to be as an N × N square array covering the field L × L, and N is odd. Then, the sample site locations in the Cartesian grid can be expressed as follows:

$$x_m = m\Delta\,,\; y_n = n\Delta \tag{2}$$

where $m = -\frac{N-1}{2}, -\frac{N-3}{2}, \cdots, \frac{N-1}{2}$, $n = -\frac{N-1}{2}, -\frac{N-3}{2}, \cdots, \frac{N-1}{2}$, and $\Delta = L/(N-1)$, which is called sample site interval. For notation simplicity, we denote as follows:

$$\begin{aligned} \mathbf{G}_{m,n} &\equiv G_{x,m,n}\mathbf{e}_x + G_{y,m,n}\mathbf{e}_y \\ G_{x,m,n} &\equiv G_x(x_m, y_n) \\ G_{y,m,n} &\equiv G_y(x_m, y_n) \end{aligned} \tag{3}$$

Figure 2(1) shows an example of the stage error, $G_{m,n}$ which leads the distortion of the actual measurement system. The objective of self-calibration in this chapter was to calculate $\mathbf{G}_{m,n}$ out which can be directly utilized to compensate the measurement accuracy. According to the presentation of [20], there are three properties for $\mathbf{G}_{m,n}$ those essentially define the ideal calibration coordinates.

- $\mathbf{G}_{m,n}$ has no translation, i.e.,

$$\sum_{m,n} G_{x,m,n} = \sum_{m,n} G_{y,m,n} = 0 \tag{4}$$

- $\mathbf{G}_{m,n}$ has no rotation, i.e.,

$$\sum_{m,n} (G_{y,m,n} x_m - G_{x,m,n} y_n) = 0 \tag{5}$$

- $\mathbf{G}_{m,n}$ has no magnification, i.e.,

$$\sum_{m,n} (G_{x,m,n} x_m + G_{y,m,n} y_n) = 0 \tag{6}$$

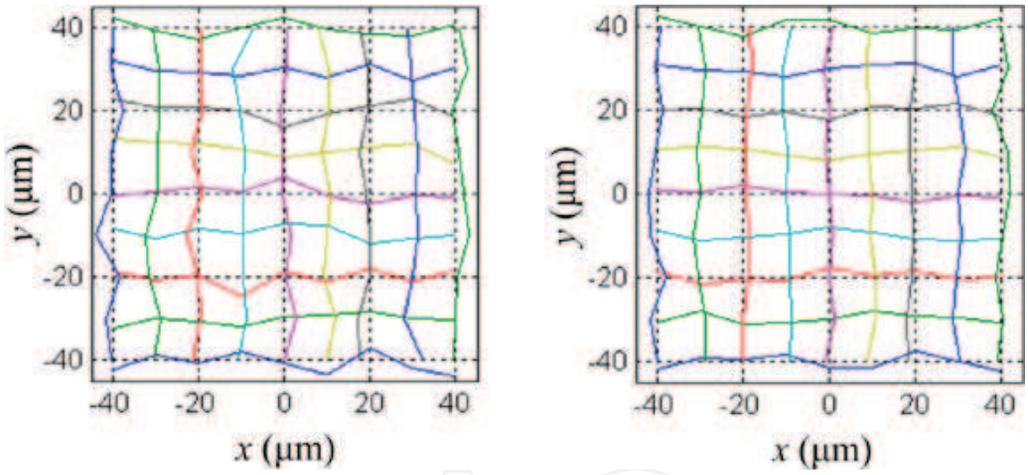

Figure 2. (1) An example of $\mathbf{G}_{m,n}$; (2) an example of $\mathbf{A}_{m,n}$.

Meanwhile, two dimensionless parameters *O* and *R* are defined as the X–Y non-orthogonality and the X–Y scale difference of $\mathbf{G}_{m,n,}$ respectively. Consequently, $\mathbf{G}_{m,n}$ be described as follows [20]:

$$\begin{aligned} G_{x,m,n} &= Oy_n + Rx_m + F_{x,m,n} \\ G_{y,m,n} &= Ox_m - Ry_n + F_{y,m,n} \end{aligned} \tag{7}$$

Therefore, the determination of $\mathbf{G}_{m,n}$ can be completed by calculating out the first-order components *O* and *R*, and the residual error $\mathbf{F}_{m,n}$. It must be noted that the origin of X–Y axis is the center of the sample array and the following properties of $\mathbf{F}_{m,n}$ could be obtained [20]:

$$\sum_{m,n} F_{x,m,n} = \sum_{m,n} F_{x,m,n} x_m = \sum_{m,n} F_{x,m,n} y_n = 0$$
$$\sum_{m,n} F_{y,m,n} = \sum_{m,n} F_{y,m,n} x_m = \sum_{m,n} F_{y,m,n} y_n = 0 \quad (8)$$

2.2. Artifact error

As we state previously, an artifact plate is needed as a critical device for the self-calibration. The used artifact plate has a square N × N mark array with the same size of the stage sample site array, and the origin of the plate X–Y axis is located at the center of the mark array. The plate axis is fixed on the plate and will move with the plate during its motion. The nominal mark locations in the plate coordinate system are the same as the sample site locations in the stage coordinate system. It is well known that the artifact plate cannot be perfect, and each actual mark at (m,n) deviates from its nominal location by $A_{m,n}$. Herein, $A_{m,n}$ is named as artifact error with one example illustrated in **Figure 2(2)**, and

$$\mathbf{A}_{m,n} \equiv A_{x,m,n}\mathbf{e}_{px} + A_{y,m,n}\mathbf{e}_{py}$$
$$A_{x,m,n} \equiv A_x(x_m, y_n) \quad (9)$$
$$A_{y,m,n} \equiv A_y(x_m, y_n)$$

where $m = -\frac{N-1}{2}, -\frac{N-3}{2}, \ldots, \frac{N-1}{2}$, $n = -\frac{N-1}{2}, -\frac{N-3}{2}, \ldots, \frac{N-1}{2}$, $\mathbf{e}_{px}$ and $\mathbf{e}_{py}$ are the unit vectors of the plate axes. It should be noted that each mark on the artifact plate is with an identification number (m,n). The mark's identification number is fixed with the mark and does not change when the plate moves on the stage. The mark number is utilized to identify each physical mark of the plate, when different measurement views are conducted and compared. Similar to the stage error $\mathbf{G}_{m,n,}$ the artifact error $\mathbf{A}_{m,n}$ also has two properties as follows [20]:

- $\mathbf{A}_{m,n}$ has no translation, i.e.,

$$\sum_{m,n} A_{x,m,n} = \sum_{m,n} A_{y,m,n} = 0 \quad (10)$$

- $\mathbf{A}_{m,n}$ has no rotation, i.e.,

$$\sum_{m,n} (A_{y,m,n} x_m - A_{x,m,n} y_n) = 0 \quad (11)$$

3. Fundamental of X–Y self-calibration

The self-calibration requires performing independent measurement views with different permutations of the artifact plate on the un-calibrated metrology stage as illustrated in

http://dx.doi.org/10.5772/62761

Figure 3, where the grid is the artifact plate and the colorful plane out of the grid is the metrology stage. The first view is the original orientation of the artifact plate referred to as View 0, in which the X-axis and Y-axis of the plate are aligned with those of the stage as closely as possible. In View 1, the artifact plate is rotated 90° around the origin from View 0 on the metrology stage. In View 2, the artifact plate is translated from the original View 0 by one sampling site + Δ along X-axis. In the following, we measure the rigid artifact plate marks when the plate is placed on the metrology stage in three measurement views. Through these measurement data, the stage error map can be determined by comparing different measurement views, and the misalignment error can be directly figured out with mathematical manipulations in detail.

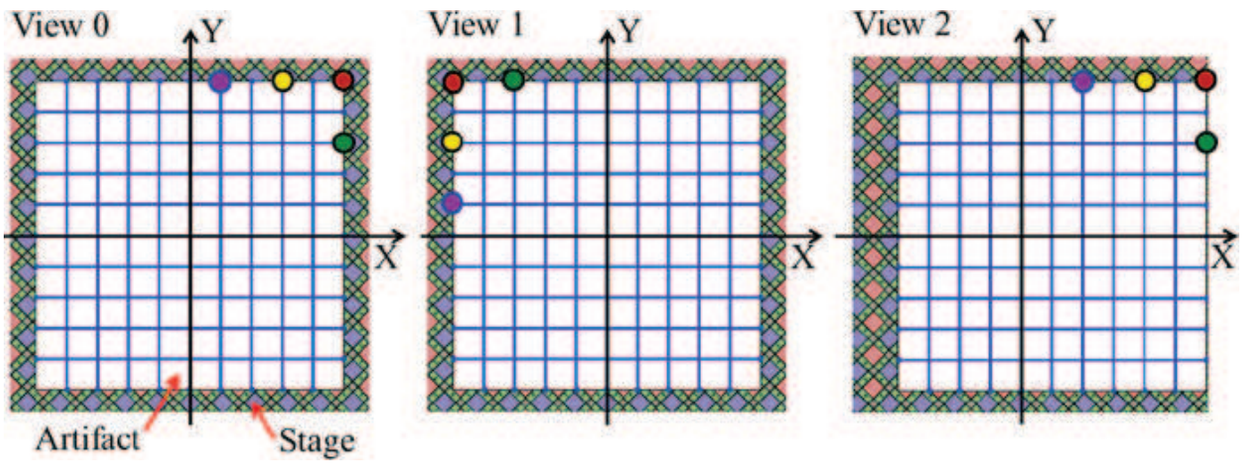

Figure 3. Three measurement views for X–Y self-calibration.

3.1. View 0

In the first view, the artifact plate is placed on the un-calibrated metrology stage with the corresponding axes aligned roughly as shown in View 0 of **Figure 3**. The deviation of mark (m,n) from the measurement value to its nominal position in the stage coordinate system is denoted as $\mathbf{v}_{0,m,n}$, where subscript 0 represents View 0. Define

$$\mathbf{v}_{0,m,n} = v_{0,x,m,n}\mathbf{e}_x + v_{0,y,m,n}\mathbf{e}_y \tag{12}$$

It must be noted that the alignment between the stage axes and plate axes cannot be perfect, i.e., there inevitably exists a small offset between their origins and a small rotation between their orientations. Therefore,

$$\begin{aligned} v_{0,x,m,n} &= G_{x,m,n} + A_{x,m,n} + E_{0,x,m,n} + r_{0,x,m,n} \\ v_{0,y,m,n} &= G_{y,m,n} + A_{y,m,n} + E_{0,y,m,n} + r_{0,y,m,n} \end{aligned} \tag{13}$$

where the misalignment error $\mathbf{E}_{0,m,n}$ is denoted as follows:

$$\begin{aligned} E_{0,x,m,n} &= -\theta_0 y_n + t_{0x} \\ E_{0,y,m,n} &= \theta_0 x_m + t_{0y} \end{aligned} \tag{14}$$

and θ_0 and $\mathbf{t}_0$ are the rotation and offset of the misalignment. $r_{0,y,m,n}$ and $r_{0,y,m,n}$are the random measurement noises. To attenuate the effects of $r_{0,x,m,n}$and $r_{0,y,m,n}$, repeated measurements are constructed with exactly the same mark position of the artifact plate. Resultantly, $V_{0,x,m,n}$ and $V_{0,y,m,n}$ are the mean values of a number of repeated measurements of $V_{0,x,m,n}$ and $V_{0,y,m,n}$, and the random measurement noise is consequently assumed to be completely attenuated, i.e.,

$$\begin{aligned} V_{0,x,m,n} &= G_{x,m,n} + A_{x,m,n} + E_{0,x,m,n} \\ V_{0,y,m,n} &= G_{y,m,n} + A_{y,m,n} + E_{0,y,m,n} \end{aligned} \tag{15}$$

Substituting Eqs. (7) and (14) into Eq. (15) leads to the following:

$$\begin{aligned} V_{0,x,m,n} &= F_{x,m,n} + Oy_n + Rx_m + A_{x,m,n} - \theta_0 y_n + t_{0x} \\ V_{0,y,m,n} &= F_{y,m,n} + Ox_m - Ry_n + A_{y,m,n} + \theta_0 x_m + t_{0y} \end{aligned} \tag{16}$$

Noting Eqs. (8), (10), (11), and (16), t_{0x}, t_{0y}, and θ_0 of the misalignment error $\mathbf{E}_{0,m,n}$ are determined [20], i.e.,

$$t_{0x} = \frac{\sum_{m,n} V_{0,x,m,n}}{N^2}, t_{0y} = \frac{\sum_{m,n} V_{0,y,m,n}}{N^2}, \theta_0 = \frac{\sum_{m,n} (V_{0,y,m,n} x_m - V_{0,x,m,n} y_n)}{\sum_{m,n} (x_m^2 + y_n^2)} \tag{17}$$

After computing $\mathbf{t}_0$ and θ_0, the misalignment error $\mathbf{E}_{0,m,n}$ is determined. Then, define

$$\begin{aligned} U_{0,x,m,n} &= V_{0,x,m,n} - t_{0x} + \theta_0 y_n \\ U_{0,y,m,n} &= V_{0,y,m,n} - t_{0y} - \theta_0 x_m \end{aligned} \tag{18}$$

It must be pointed out that, the transformation from $\mathbf{V}_{0,m,n}$ to $\mathbf{U}_{0,m,n}$ is commonly referred to as multiple-point alignment. Combining Eqs. (16) and (18) leads to the following

$$\begin{aligned} F_{x,m,n} + A_{x,m,n} &= U_{0,x,m,n} - Oy_n - Rx_m \\ F_{y,m,n} + A_{y,m,n} &= U_{0,y,m,n} - Ox_m + Ry_n \end{aligned} \tag{19}$$

http://dx.doi.org/10.5772/62761

3.2. View 1

In the second measurement view, the artifact plate is rotated 90° around the origin from View 0 as shown in View 1 of **Figure 3**. In this view, the plate X-axis is aligned along the stage Y-direction with same direction, and plate Y-axis is aligned along the stage X-direction but with converse direction. The deviation of mark (*m*,*n*) from the measurement value to its nominal position in the stage coordinate system is denoted as $\mathbf{V}_{1,m,n}$, where subscript 1 represents View 1. It must be noted that although located at a different position relative to the stage, the mark (*m*,*n*) in View 1 is the same physical mark (*m*,*n*) in View 0. Then,

$$\mathbf{v}_{1,m,n} = v_{1,x,m,n}\mathbf{e}_x + v_{1,y,m,n}\mathbf{e}_y \tag{20}$$

and

$$\begin{aligned} V_{1,x,m,n} &= G_{x,-n,m} - A_{y,m,n} + E_{1,x,m,n} \\ V_{1,y,m,n} &= G_{y,-n,m} + A_{x,m,n} + E_{1,y,m,n} \end{aligned} \tag{21}$$

where $\mathbf{V}_{1,m,n}$ is the mean value of a number of measurements of $\mathbf{V}_{1,m,n}$, and $\mathbf{E}_{1,m,n}$ is the misalignment error. With similar procedure of above subsection, we define

$$\begin{aligned} U_{1,x,m,n} &= V_{1,x,m,n} - \frac{\sum_{m,n} V_{1,x,m,n}}{N^2} + \frac{\sum_{m,n}(-V_{1,y,m,n}y_n - V_{1,x,m,n}x_m)}{\sum_{m,n}(x_m^2 + y_n^2)}x_m \\ U_{1,y,m,n} &= V_{1,y,m,n} - \frac{\sum_{m,n} V_{1,y,m,n}}{N^2} + \frac{\sum_{m,n}(-V_{1,y,m,n}y_n - V_{1,x,m,n}x_m)}{\sum_{m,n}(x_m^2 + y_n^2)}y_n \end{aligned} \tag{22}$$

Consequently, Eqs. (21) and (22) yield

$$\begin{aligned} F_{x,-n,m} - A_{y,m,n} &= U_{1,x,m,n} - Ox_m + Ry_n \\ F_{y,-n,m} + A_{x,m,n} &= U_{1,y,m,n} + Oy_n + Rx_m \end{aligned} \tag{23}$$

Comparing Eq. (23) of View 1 with Eq. (19) of View 0, with the same procedure in [20], the stage error components *O* and *R* can be calculated out as follows:

$$O = \frac{1}{2}\left[\frac{\sum_{m,n}(U_{0,x,m,n}y_n + U_{0,y,m,n}x_m)}{\sum_{m,n}(x_m^2 + y_n^2)} + \frac{\sum_{m,n}(U_{1,x,m,n}x_m - U_{1,y,m,n}y_n)}{\sum_{m,n}(x_m^2 + y_n^2)}\right]$$
$$R = \frac{1}{2}\left[\frac{\sum_{m,n}(U_{0,x,m,n}x_m - U_{0,y,m,n}y_n)}{\sum_{m,n}(x_m^2 + y_n^2)} + \frac{\sum_{m,n}(-U_{1,x,m,n}y_n - U_{1,y,m,n}x_m)}{\sum_{m,n}(x_m^2 + y_n^2)}\right] \quad (24)$$

After calculating out *O* and *R*, Eqs. (19) and (23) can lead to the following

$$\begin{aligned} F_{x,m,n} - F_{y,-n,m} &= P_{m,n} \\ F_{y,m,n} + F_{x,-n,m} &= Q_{m,n} \end{aligned} \quad (25)$$

where

$$\begin{aligned} P_{m,n} &= U_{0,x,m,n} - U_{1,y,m,n} - 2Oy_n - 2Rx_m \\ Q_{m,n} &= U_{0,y,m,n} + U_{1,x,m,n} - 2Ox_m + 2Ry_n \end{aligned} \quad (26)$$

3.3. View 2

As the first-order components *O* and *R* have been determined by View 0 and View 1, we try to determine $\mathbf{F}_{m,n}$ in the third view. In this view, the artifact plate is translated by roughly one sample site interval +Δ from View 0 along X-axis relative to the stage, while the stage axes and plate axes are roughly aligned, which is shown in View 2 of **Figure 3**. The deviation of mark (*m*,*n*) from the measurement value to its nominal position in the stage coordinate system is denoted as $\mathbf{v}_{2,m,n}$, where subscript 2 represents View 2. Different from View 0 and View 1, the subscript *m* here is from $-\frac{N-1}{2}$ to $-\frac{N-3}{2}$, due to that the far right column, i.e., $m = -\frac{N-1}{2}$, is outside the initial N × N stage sample sites. It also should be noted that although located at a different position relative to the stage (by about one sample site interval translation), the mark (*m*,*n*) here is the same physical mark (*m*,*n*) in View 0. As only the (N − 1) × N sites in View 2 within the initial N × N sites can be used, the properties of no translation and no rotation cannot be used.

Similar to Views 0 and 1, we can obtain

$$\mathbf{v}_{2,m,n} = v_{2,x,m,n}\mathbf{e}_x + v_{2,y,m,n}\mathbf{e}_y \quad (27)$$

and

$$\begin{aligned} V_{2,x,m,n} &= G_{x,m+1,n} + A_{x,m,n} + E_{2,x,m,n} \\ V_{2,y,m,n} &= G_{y,m+1,n} + A_{y,m,n} + E_{2,y,m,n} \\ E_{2,x,m,n} &= -\theta_2 y_n + t_{2x} \\ E_{2,y,m,n} &= \theta_2 x_m + t_{2y} \end{aligned} \tag{28}$$

where $m = -\frac{N-1}{2}, -\frac{N-3}{2}, \ldots, \frac{N-1}{2}$, $\mathbf{V}_{2,m,n}$, is the mean value of a number of measurements of, $\mathbf{V}_{2,m,n}$, θ_2 and $\mathbf{t}_2$ are the rotation and offset of the misalignment. To be consistent with the previous two views, $\mathbf{U}_{2,m,n}$ is used instead of $\mathbf{V}_{2,m,n}$, i.e.,

$$U_{2,x,m,n} = V_{2,x,m,n},\ U_{2,y,m,n} = V_{2,y,m,n} \tag{29}$$

Combining Eqs. (28) and (29) and noting $x_{m+1} = x_m + \Delta$ lead to the following

$$\begin{aligned} F_{x,m+1,n} + A_{x,m,n} &= U_{2,x,m,n} - Oy_n - Rx_m + \xi_x - \xi_\theta y_n \\ F_{y,m+1,n} + A_{y,m,n} &= U_{2,y,m,n} - Ox_m + Ry_n + \xi_y + \xi_\theta x_m \end{aligned} \tag{30}$$

where $\xi_x = -(t_{2x} + R\Delta)$, $\xi_y = -(t_{2y} + O\Delta)$, $\xi_\theta = -\theta_2$. Subtracting Eq. (19) from (30) leads to the following

$$\begin{aligned} F_{x,m+1,n} - F_{x,m,n} &= U_{2,x,m,n} - U_{0,x,m,n} + \xi_x - \xi_\theta y_n \\ F_{y,m+1,n} - F_{y,m,n} &= U_{2,y,m,n} - U_{0,y,m,n} + \xi_y + \xi_\theta x_m \end{aligned} \tag{31}$$

Unlike the cases in View 0 and View 1, the misalignment error of View 2 is not identified simply by applying the properties of $\mathbf{G}_{m,n}$, $\mathbf{F}_{m,n}$ and $\mathbf{A}_{m,n}$, as View 2 provides no measurement data for the first column of the sampling sites. Certain algebraic manipulation is needed and is explained in Appendix A, B, and C, where the full procedures to determine the misalignment error components of View 2, i.e., ξ_θ, ξ_x, and ξ_y, are separately presented in detail. It should be pointed out that the determination process of ξ_θ, ξ_x, and ξ_y also can be used as foundation for research of other self-calibration schemes.

4. Self-calibration algorithm for X–Y metrology systems

In this section, we try to synthesize a self-calibration algorithm for X–Y precision metrology stages with accuracy and simplicity orientation. The proposed method should be well understood and robust to meet the challenge of random measurement noise, which are both important for engineers to implement in practical applications. In the following, two schemes are provided.

4.1. Scheme I

Combining Eqs. (25), (31), and (8), the following equation group for $F_{x,m,n}$ and $F_{y,m,n}$ can be obtained:

$$\begin{aligned}
&F_{x,m,n} - F_{y,-n,m} = U_{0,x,m,n} - U_{1,y,m,n} - 2Oy_n - 2Rx_m \\
&F_{y,m,n} + F_{x,-n,m} = U_{0,y,m,n} + U_{1,x,m,n} - 2Ox_m + 2Ry_n \\
&F_{x,m+1,n} - F_{x,m,n} = U_{2,x,m,n} - U_{0,x,m,n} + \xi_x - \xi_\theta y_n \\
&F_{y,m+1,n} - F_{y,m,n} = U_{2,y,m,n} - U_{0,y,m,n} + \xi_y + \xi_\theta x_m \\
&\sum_{m,n} F_{x,m,n} = \sum_{m,n} F_{x,m,n} x_m = \sum_{m,n} F_{x,m,n} y_n = 0 \\
&\sum_{m,n} F_{y,m,n} = \sum_{m,n} F_{y,m,n} x_m = \sum_{m,n} F_{y,m,n} y_n = 0
\end{aligned} \tag{32}$$

Eq. (32) actually supplies linear equations for calculation of $F_{x,m,n}$ and $F_{y,m,n}$ with certain redundancy. Therefore, a least-square solution for $\mathbf{F}_{m,n}$ can be synthesized with robustness to meet the challenge of random measurement noise. To provide a more explicit illustration, we take $N = 11$ as an example, and Eq. (32) can then be assembled into matrix form, i.e., $ME_F = S$, where M is a relational matrix of dimension 468 × 242, E_F is a vector of dimension 242 × 1, and S is a vector of dimension 468 × 1. This assembly of equations under matrix form is as follows:

$$ME_F = S \tag{33}$$

where

$$\begin{aligned}
E_F = [&F_{x,-5,-5}, F_{x,-4,-5}, F_{x,-3,-5}, \ldots, F_{x,5,-5}, \\
&F_{x,-5,-4}, F_{x,-4,-4}, F_{x,-3,-4}, \ldots, F_{x,5,-4}, \\
&\vdots \\
&F_{x,-5,5}, F_{x,-4,5}, F_{x,-3,5}, \ldots, F_{x,5,5}, \\
&F_{y,-5,-5}, F_{y,-4,-5}, F_{y,-3,-5}, \ldots, F_{y,5,-5}, \\
&F_{y,-5,-4}, F_{y,-4,-4}, F_{y,-3,-4}, \ldots, F_{y,5,-4}, \\
&\vdots \\
&F_{y,-5,5}, F_{y,-4,5}, F_{y,-3,5}, \ldots, F_{y,5,5}]^T_{242\times 1}
\end{aligned} \tag{34}$$

We have stated previously that three measurement views are required to generate equations with data redundancy. Consequently, a least-square method can be synthesized to provide a solution as follows

$$E_F = (M^T M)^{-1} M^T S \tag{35}$$

which possesses certain robustness to random measurement noise. Therefore, $\mathbf{F}_{m,n}$ is obtained which leads to the final determination of $G_{m,n}$.

4.2. Scheme II

As presented above, with the determination of the misalignment errors detailed in the Appendix, the stage error can be calculated out. However, it also can be observed from the Appendix that the computation process is complicated to some extent. Herein, this chapter also analyses the necessity of this costly computation and provides another alternative as follows [22].

As ξ_θ can be calculated out in the Appendix, define:

$$\begin{aligned} L_{x,m,n} &= U_{2,x,m,n} - U_{0,x,m,n} - \xi_\theta y_n \\ L_{y,m,n} &= U_{2,y,m,n} - U_{0,y,m,n} + \xi_\theta x_m \end{aligned} \tag{36}$$

Combining (31) and (36) leads to the following

$$\begin{aligned} &F_{x,m+2,n} - 2F_{x,m+1,n} + F_{x,m,n} = L_{x,m+1,n} - L_{x,m,n} \\ &F_{x,m+1,n+1} - F_{x,m+1,n} - F_{x,m,n+1} + F_{x,m,n} = L_{x,m,n+1} - L_{x,m,n} \\ &F_{y,m+2,n} - 2F_{y,m+1,n} + F_{y,m,n} = L_{y,m+1,n} - L_{y,m,n} \\ &F_{y,m+1,n+1} - F_{y,m+1,n} - F_{y,m,n+1} + F_{y,m,n} = L_{y,m,n+1} - L_{y,m,n} \end{aligned} \tag{37}$$

Consequently, the equations for $\mathbf{F}_{m,n}$ from (8), (25), and (37) can be grouped as follows

$$\begin{aligned} &\sum_{m,n} F_{x,m,n} = \sum_{m,n} F_{x,m,n} x_m = \sum_{m,n} F_{x,m,n} y_n = 0 \\ &\sum_{m,n} F_{y,m,n} = \sum_{m,n} F_{y,m,n} x_m = \sum_{m,n} F_{y,m,n} y_n = 0 \\ &F_{x,m,n} - F_{y,-n,m} = P_{m,n} \\ &F_{y,m,n} + F_{x,-n,m} = Q_{m,n} \\ &F_{x,m+2,n} - 2F_{x,m+1,n} + F_{x,m,n} = L_{x,m+1,n} - L_{x,m,n} \\ &F_{x,m+1,n+1} - F_{x,m+1,n} - F_{x,m,n+1} + F_{x,m,n} = L_{x,m,n+1} - L_{x,m,n} \\ &F_{y,m+2,n} - 2F_{y,m+1,n} + F_{y,m,n} = L_{y,m+1,n} - L_{y,m,n} \\ &F_{y,m+1,n+1} - F_{y,m+1,n} - F_{y,m,n+1} + F_{y,m,n} = L_{y,m,n+1} - L_{y,m,n} \end{aligned} \tag{38}$$

Eq. (38) also provides linear equations for determination of $F_{x,m,n}$ and $F_{y,m,n}$ with certain redundancy. Then, a least-square solution for $\mathbf{F}_{m,n}$ can be synthesized. In detail, Eq. (38) can be assembled into matrix form as follows

$$\Gamma E_F = S \tag{39}$$

where **Γ** is a relational matrix of dimension $D_1 \times D_2$, E_F is a vector of dimension $D_2 \times 1$, and S is a vector of dimension $D_1 \times 1$. Noting the subscripts of (38), we can calculate out D_1 and D_2 as: $D_1 = 6 + N^2 + N^2 + (N-2) \times N + (N-1)^2 + (N-2) \times N + (N-1)^2 = 6N^2 - 8N + 8$, $D_2 = N^2 + N^2 = 2N^2$. For example, assuming $N = 11$, Γis of dimension 646 × 242 which can be determined by (38), while

$$\begin{aligned}
E_F = [&F_{x,-5,-5}, F_{x,-4,-5}, F_{x,-3,-5}, \ldots, F_{x,5,-5},\\
&F_{x,-5,-4}, F_{x,-4,-4}, F_{x,-3,-4}, \ldots, F_{x,5,-4},\\
&\vdots\\
&F_{x,-5,5}, F_{x,-4,5}, F_{x,-3,5}, \ldots, F_{x,5,5},\\
&F_{y,-5,-5}, F_{y,-4,-5}, F_{y,-3,-5}, \ldots, F_{y,5,-5},\\
&F_{y,-5,-4}, F_{y,-4,-4}, F_{y,-3,-4}, \ldots, F_{y,5,-4},\\
&\vdots\\
&F_{y,-5,-3}, F_{y,-4,-3}, F_{y,-3,-3}, \ldots, F_{y,5,-3},\\
S = [&0,0,0,0,0,0, P_{-5,-5}, P_{-4,-5}, \ldots, P_{5,5},\\
&Q_{-5,-5}, Q_{-4,-5}, Q_{-3,-5}, Q_{-2,-5}, \ldots, Q_{5,5},\\
&L_{x,-4,-5} - L_{x,-5,-5}, \ldots, L_{x,5,5} - L_{x,4,5},\\
&\vdots\\
&L_{y,-5,-4} - L_{x,-5,-5}, \ldots, L_{x,5,5} - L_{x,5,4}]^T_{646\times 1}
\end{aligned} \tag{40}$$

As the system has requisite data redundancy, it can be solved using a least-square method to calculate $F_{x,m,n}$ and $F_{y,m,n}$, producing a solution like

$$E_F = (\Gamma^T \Gamma)^{-1} \Gamma^T S \tag{41}$$

Therefore, $\mathbf{F}_{m,n}$ is obtained with certain robustness which finally leads to the determination of $\mathbf{G}_{m,n}$ by (7) as O and R are all known.

It should be pointed out that the proposed scheme does not calculate out the misalignment error components ξ_x and ξ_y, while these calculations are important in previous published strategies [15, 23, 24]. The proposed scheme does not need this costly computation, which would be meaningful for simplification of the calculation process to some extent. In the reminder of this chapter, as Scheme I is a holistic method and Scheme II is a simplified alternative, the simulation test and self-calibration procedure are all presented just for Scheme I. Readers could follow the following presentation to conduct similar issues for Scheme II.

http://dx.doi.org/10.5772/62761

5. Computer simulation

In the following, the proposed self-calibration scheme would be tested by simulation. The stage error is assumed to be on a 11 × 11 sample site array with the sample site internal Δ = 10 mm. And the stage error is generated by the command "normrnd" of MATLAB software with mean of 0 and standard deviation of 0.3, plus certain sine/cosine functions which may be partial characteristics of the stage error data, i.e.,

$$\begin{aligned} G_{x,m,n} &= normrnd(0,0.3,11,11) + 0.5sin(3m \times \frac{2\pi}{11}) \\ G_{y,m,n} &= normrnd(0,0.3,11,11) + 0.5cos(3n \times \frac{2\pi}{11}) \end{aligned} \tag{42}$$

The above data are utilized as the nominal $G_{m,n}$ shown in **Figure 4**, where the red vector lines are the stage error which have been zoomed in for 5000 times. It must be noted that $G_{x,m,n}$ and $G_{y,m,n}$ are both generated by *normrnd* (0, 0.3, 11, 11), respectively. To satisfy relevant constrains such as Eq. (4), little data modification has been made. In addition, the artifact error including $\mathbf{A}_{x,m,n}$and $\mathbf{A}_{y,m,n}$ is generated with mean of 0 and standard deviation of 0.5 μm.

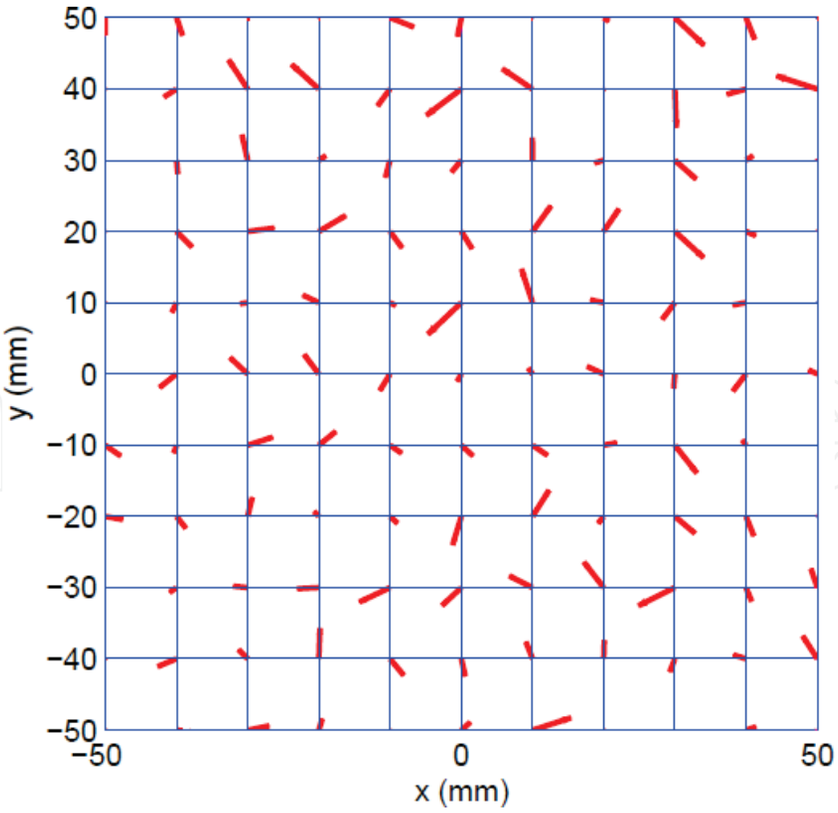

Figure 4. Nominal $\mathbf{G}_{m,n}$ × 5000 with max($\mathbf{G}_{m,n}$) = = 1.0832 μm, min($\mathbf{G}_{m,n}$) = − 1.1448 μm, and std($\mathbf{G}_{m,n}$) = 0.4611 μm.

5.1. Case I: simulation without random measurement noise

In this subsection, the random measurement noise is assumed to be perfectly compensated by the mean value of a number of repeated measurements. The recalculated stage error $\widehat{\mathbf{G}}_{m,n,}$ i.e., $\hat{G}_{x,m,n}$ and $\hat{G}_{y,m,n}$, can be calculated out through the proposed self-calibration strategy. **Figure 5** illustrates the calibration error $\boldsymbol{E}_G$ including E_{Gx} and E_{Gy}, i.e., $\boldsymbol{E}_G = \boldsymbol{G}_{m,n} - \widehat{\mathbf{G}}_{m,n,}\, E_{Gx} = G_{x,m,n} - \hat{G}_{x,m,n}$and $E_{Gy} = G_{y,m,n} - \hat{G}_{y,m,n}$. The calibration error is shown as the red vector lines those have been zoomed in for 5 × 10^{17} times. The maximum value $max(\cdot)$, the minimum value $min(\cdot)$ and the standard deviation $std(\cdot)$of $\boldsymbol{G}_{m,n}$ $\widehat{\mathbf{G}}_{m,n}$ and $\boldsymbol{E}_G$ are all listed in **Table 1**. It can be observed that the reconstructed stage error $\widehat{\mathbf{G}}_{m,n}$ is always quite close to the actual stage error $\widehat{\mathbf{G}}_{m,n,}$ and the calibration errors are all below 1.6 × 10^{-14} μm , which validate that the proposed self-calibration algorithm can accurately determine the stage error without the existence of random measurement noise.

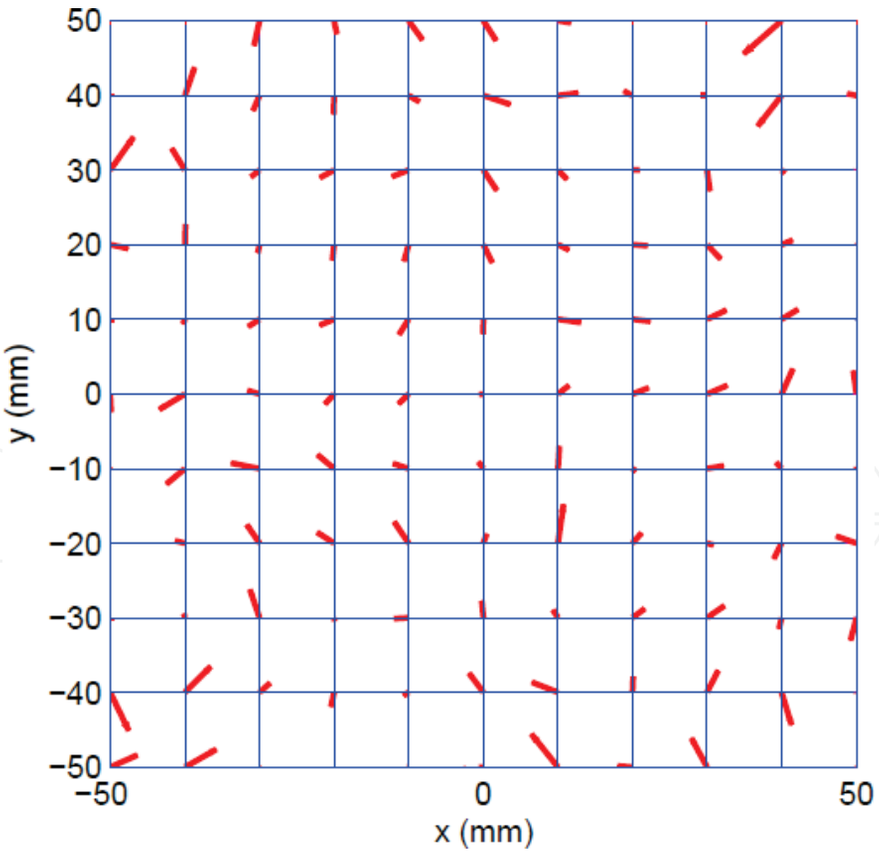

Figure 5. Calibration error $E_{Gy}(\mu m)$s × 5 × 10^{17} with max(E_G) = 1.5127 × 10^{-14}μm, min(E_G) = −1.1546 × 10^{-14}μm, and std(E_G) = 4.6547 × 10^{-15}μm (without random measurement noise).

http://dx.doi.org/10.5772/62761

	max (·)	min (·)	std (·)
$G_{mn}(\mu\text{m})$	1.0832	−1.1448	0.4611
$G_{x,m,n}(\mu\text{m})$	1.0832	−1.1448	0.4659
$G_{y,m,n}(\mu\text{m})$	0.9753	−1.0870	0.4583
$\widehat{G}_{m,n}(\mu\text{m})$	1.0832	−1.1448	0.4611
$\widehat{G}_{x,m,n}(\mu\text{m})$	1.0831	−1.1448	0.4659
$\widehat{G}_{y,m,n}(\mu\text{m})$	0.9753	−1.0870	0.4583
$E_G(\mu\text{m})$	1.5127×10^{-14}	-1.1546×10^{-14}	4.6547×10^{-15}
$E_{Gx}(\mu\text{m})$	1.2046×10^{-14}	-1.0214×10^{-14}	4.3670×10^{-15}
$E_{Gy}(\mu\text{m})$	1.5127×10^{-14}	-1.1546×10^{-14}	4.9431×10^{-15}

Table 1. Calculation performance indexes (without random measurement noise).

5.2. Case II: simulation with random measurement noise of standard deviation 0.05 μm

The nominal stage error and artifact error in this subsection keep same with those of Section 5.1, except that in all site's measurements, we add independent random Gaussian measurement noises. The random measurement noise is generated with mean of 0 and standard deviation of $0.05\mu m$. Following the proposed self-calibration scheme, the reconstructed stage error $\widehat{\mathbf{G}}_{m,n}$, i.e., $\widehat{G}_{x,m,n}$ and $\widehat{G}_{y,m,n}$ also can be computed out. The calibration error E_G, which is the difference between the recalculated and the actual stage error, is shown in **Figure 6**, where the red vector lines as E_G have been zoomed in for 5×10^4 times. The maximum value $max(\cdot)$, the minimum value $max(\cdot)$, and the standard deviation of $G_{x,m,n}$, $G_{y,m,n}$, E_{Gx}, and E_{Gy} are all listed in **Table 2**. It can be seen that the proposed self-calibration method

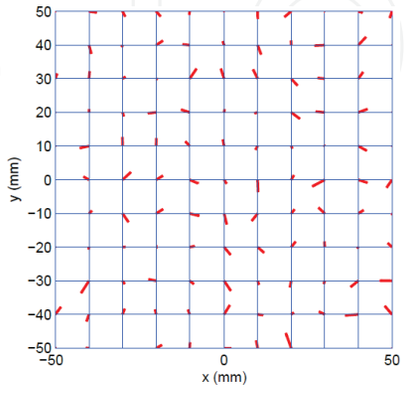

Figure 6. Calibration error $E_G \times 5 \times 10^4$ with $\max(E_G) = 0.0899$ μm, $\min(E_G) = -0.0793$ μm and $\text{std}(E_G) = 0.0334$ μm (with random measurement noise std = 0.05 μm).

can determine the stage error rather exactly even there exists certain random measurement noise —when the measurement noise is with standard deviation of 0.05 μm , the corresponding calibration error is with a standard deviation of 0.0334 μm which is at the same level as the random measurement noise.

We also further test the calculation robustness of the proposed scheme to various random measurement noises those are continuously generated by arbitrary 15 times. The standard deviations of the resultant calibration errors are shown in **Figure 7**, where the 15 standard deviations are all below 0.05 μm . These results consistently validate that the proposed self-calibration algorithm can meet the challenge of random measurement noise effectively.

	max (·)	**min (·)**	**std (·)**
$\hat{G}_{m,n}(\mu\text{m})$	1.0919	−1.1598	0.4645
$\hat{G}_{x,m,n}(\mu\text{m})$	1.0919	−1.1598	0.4693
$\hat{G}_{y,m,n}(\mu\text{m})$	0.9744	−1.0835	0.4617
$E_G(\mu\text{m})$	0.0899	−0.0793	0.0334
$E_{Gx}(\mu\text{m})$	0.0552	−0.0793	0.0334
$E_{Gy}(\mu\text{m})$	0.0899	−0.0759	0.0336

Table 2. Calculation performance indexes (with random measurement noise std = 0.05 μm).

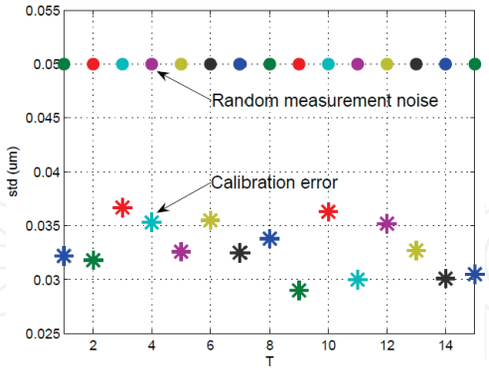

Figure 7. Standard deviation of calibration error for arbitrary 15 times (with random measurement noise std = 0.05 μm).

5.3. Case III: simulation with random measurement noise of standard deviation 5×10^{-4} μm

In this subsection, we implement other simulation to test the consistency of the proposed scheme to random measurement noise. The random measurement noise is generated with mean of 0 and standard deviation of 0.0005 μm which is rather small. **Figure 8** shows the

http://dx.doi.org/10.5772/62761

resultant calibration error $\boldsymbol{E}_G$ under the existence of random measurement noise, where the red vector lines is $\boldsymbol{E}_G$ which have been zoomed in for 5×10^6 times. The maximum value $max(\cdot)$, the minimum value $min(\cdot)$, and the standard deviation $std(\cdot)$ of $G_{x,m,n}$, $G_{y,m,n}$, E_{Gx} and E_{Gy} are all listed in **Table 3**. Seen from this table, the proposed method can determine the stage error when there exists random measurement noise with standard deviation of 0.0005 μm --- —the standard deviation of calibration error is about 0.000327 μm , again the same level as the random measurement noise. The algorithm's robustness is further tested for arbitrary 15 times with standard deviation of 0.0005 μm , and **Figure 9** shows the standard deviations of the calibration errors. It can be seen from the figure that the standard deviations are all <0.0005 μm . All these results consistently validate that the proposed self-calibration algorithm can compute the stage error rather accurately no matter what the random measurement noise is.

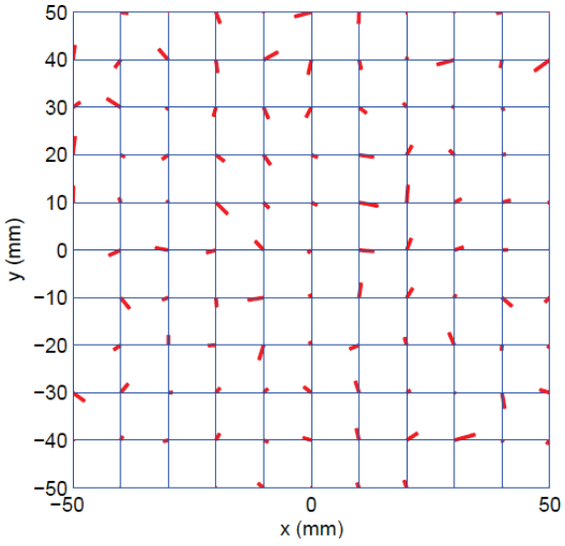

Figure 8. Calibration error $E_G \times 5 \times 10^6$ with $\max(E_G) = 8.8410 \times 10^{-4}$ μm, $\min(E_G) = -7.4194 \times 10^{-4}$ μm and $\text{std}(E_G) = 3.2684 \times 10^{-4}$ μm (with random measurement noise std = 5×10^{-4} μm).

	max (·)	**min (·)**	**std (·)**
$\hat{G}_{m,n}(\mu\text{m})$	1.0833	−1.1441	0.4612
$\hat{G}_{x,m,n}(\mu\text{m})$	1.0833	−1.1441	0.4659
$\hat{G}_{y,m,n}(\mu\text{m})$	0.9756	−1.0868	0.4583
$E_G(\mu\text{m})$	8.8410×10^{-4}	-7.4194×10^{-4}	3.2684×10^{-4}
$E_{Gx}(\mu\text{m})$	8.8410×10^{-4}	-7.4194×10^{-4}	3.2804×10^{-4}
$E_{Gy}(\mu\text{m})$	7.8703×10^{-4}	-6.6555×10^{-4}	3.2700×10^{-4}

Table 3. Calculation performance indexes (with random measurement noise std = 5×10^{-4} μm).

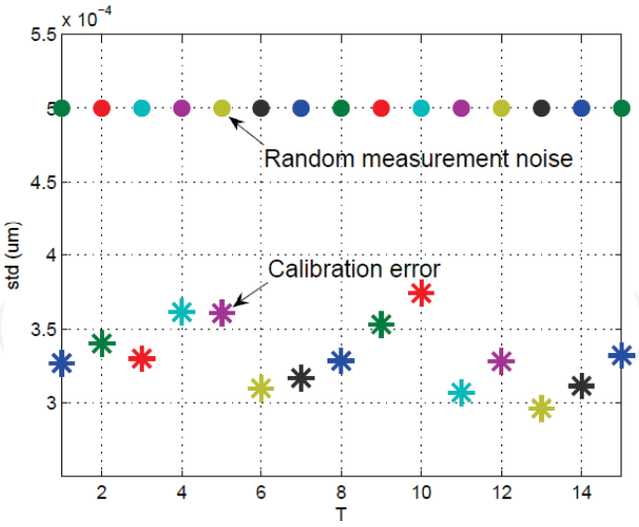

Figure 9. Standard deviation of calibration error for arbitrary 15 times (with random measurement noise std = 5×10^{-4} μm).

6. Standard self-calibration procedure

In this section, the procedure of performing a standard self-calibration following the proposed scheme is provided to facilitate practical implementations. To illustrate the procedure more clearly, a self-calibration system including an artifact plate, a two-dimensional stage, and a mark alignment system is developed and shown in **Figure 10**. Herein, the mark alignment system is developed to precisely obtain the measurement information of each mark position. The actual steps are listed in the following.

- Step 0: Place the artifact plate on the 2-D metrology stage as shown in View 0 of **Figure 1**. Utilize the metrology stage to measure the marks of the artifact plate through the mark alignment system. Obtain $v_{0,x,m,n}$ and $v_{0,y,m,n}$ for K (e.g. $K = 10$) times, and get $U_{0,x,m,n}$ and $U_{0,y,m,n}$ by (18), respectively.
- Step 1: Place the artifact plate on the 2-D metrology stage as shown in View 1 of **Figure 1**. Use the metrology stage to measure the marks of the artifact plate, and get $v_{1,x,m,n}$ and $v_{1,y,m,n}$ for K (e.g. $K = 10$) times. Then, determine $U_{1,x,m,n}$ and $U_{1,y,m,n}$ by (22), and obtain O and R by (24).
- Step 2: Place the artifact plate on the 2-D metrology stage as shown in View 2 of **Figure 1**. Use the metrology stage to measure the marks of the artifact plate, and get $v_{2,x,m,n}$ and $v_{2,y,m,n}$ for K (e.g. $K = 10$) times. Compute the misalignment error components ξ_θ, ξ_x, ξ_y , and obtain (31).
- Step 3: Through above steps, Eq. (32) can be consequently obtained. Then, by (35), $F_{x,m,n}$ and $F_{y,m,n}$ can be figured out. Finally, $G_{x,m,n}$ and $G_{y,m,n}$ can be computed out by (7) as O and R are previously determined by Step 1.

http://dx.doi.org/10.5772/62761

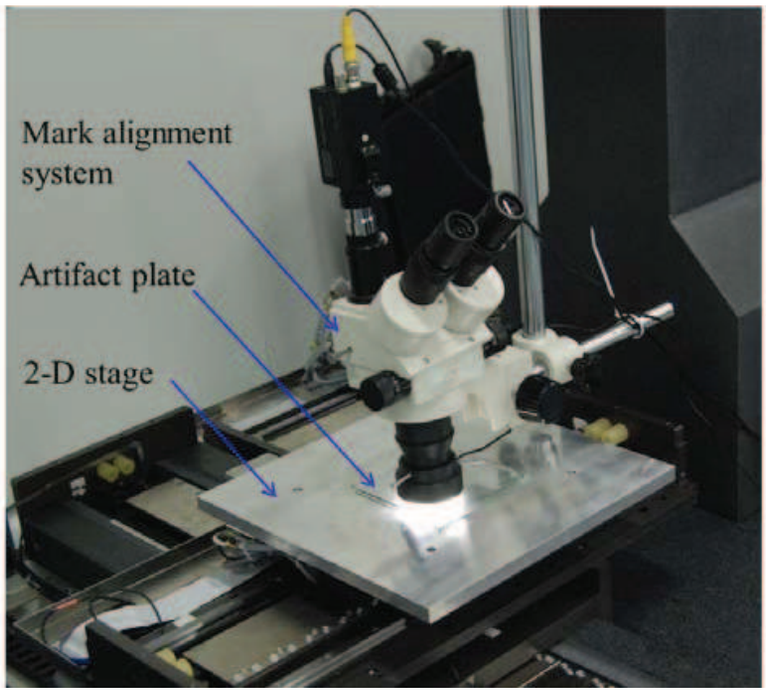

Figure 10. An example setup for 2-D self-calibration.

7. Conclusions

In this chapter, a least-square-based self-calibration strategy with simplicity and accuracy orientation has been proposed for two-dimensional precision metrology stages to address the measurement accuracy calibration problem. Three measurement views of an artifact plate on the un-calibrated metrology stage are utilized to construct symmetry, transitivity, and redundancy of the stage error, which is the basis for the synthesis of a least-square-based self-calibration algorithm. The misalignment error of each measurement view has been calculated out with explicit mathematical manipulations, while the necessity of these costly computations has been discussed. The proposed algorithm has been investigated by computer simulation, and the results show that the self-calibration strategy can reconstruct the stage error map rather precisely even there exist various random measurement noises. Finally, the procedure for performing the proposed self-calibration has been presented for engineers to facilitate practical implementation.

Acknowledgements

This work is supported by National Nature Science Foundation of China (Grant 51475262) and Autonomous Scientific Research Project of Tsinghua University (Grant 20151080363).

Appendix

Appendix A

Calculation of misalignment error component ξ_θ : Through Eq. (**31**), one can get

$$\begin{aligned}&(F_{x,m+1,n}+F_{x,-(m+1),-n})-(F_{x,m,n}+F_{x,-m,-n})\\&=(F_{x,m+1,n}-F_{x,m,n})-(F_{x,-m,-n}-F_{x,-(m+1),-n})\\&=U_{2,x,m,n}-U_{0,x,m,n}+\xi_x-\xi_\theta y_n-(U_{2,x,-(m+1),-n}-U_{0,x,-(m+1),-n}+\xi_x-\xi_\theta y_{-n})\\&=(U_{2,x,m,n}-U_{0,x,m,n}-U_{2,x,-(m+1),-n}+U_{0,x,-(m+1),-n})-\xi_\theta(y_n-y_{-n})\end{aligned} \tag{43}$$

Changing the index of Eq. (25), we can obtain

$$\begin{aligned}F_{x,-m,-n}+F_{y,-n,m}&=Q_{-n,m}\\F_{x,-n,m}-F_{y,-m,-n}&=P_{-n,m}\end{aligned} \tag{44}$$

Combining Eqs. (25) and (44) leads to the following

$$\begin{aligned}F_{x,m,n}+F_{x,-m,-n}&=C_{m,n}\equiv P_{m,n}+Q_{-n,m}\\F_{y,m,n}+F_{y,-m,-n}&=D_{m,n}\equiv Q_{m,n}-P_{-n,m}\end{aligned} \tag{45}$$

Then, noting Eqs. (43) and (45), we can obtain

$$(U_{2,x,m,n}-U_{0,x,m,n}-U_{2,x,-(m+1),-n}+U_{0,x,-(m+1),-n})-\xi_\theta(y_n-y_{-n})=C_{m+1,n}-C_{m,n} \tag{46}$$

Eq. (46) can be directly utilized to determine the value of ξ_θ.

Appendix B

Calculation of misalignment error component ξ_x : Summing Eq. (31) over n leads to the following

$$\begin{aligned}H_{x,m+1}-H_{x,m}&=Z_{x,m}+N\xi_x\\H_{y,m+1}-H_{y,m}&=Z_{y,m}+N\xi_y+N\xi_\theta x_m\end{aligned} \tag{47}$$

where $m=-\frac{N-1}{2},\ \cdots,\ \frac{N-3}{2}$, and

$$\begin{aligned} H_{x,m} &= \sum_n F_{x,m,n}, Z_{x,m} = \sum_n (U_{2,x,m,n} - U_{0,x,m,n}) \\ H_{y,m} &= \sum_n F_{y,m,n}, Z_{y,m} = \sum_n (U_{2,y,m,n} - U_{0,y,m,n}) \end{aligned} \tag{48}$$

Considering $H_{x,m}$, with $j = -\frac{N-1}{2}$, we can obtain

$$\begin{aligned} &\sum_{m=-j}^{j} H_{x,m} x_m \\ &= H_{x,-j} x_{-j} + \{[H_{x,-j+1} - H_{x,-j}] + H_{x,-j}\} x_{-j+1} + \ldots \\ &\quad + \{[H_{x,j} - H_{x,j-1}] + [H_{x,j-1} - H_{x,j-2}] \quad + [H_{x,j-2} - H_{x,j-3}] + \ldots + H_{x,-j}\} x_j \\ &= H_{x,-j} \sum_{m=-j}^{j} x_m + [H_{x,-j+1} - H_{x,-j}] \sum_{m=-j+1}^{j} x_m + \ldots + [H_{x,j} - H_{x,j-1}] \sum_{m=j}^{j} x_m \end{aligned} \tag{49}$$

Substituting (47) into (49), and noting $\sum_{m=-j}^{j} x_m = 0$, one can get

$$\begin{aligned} &\sum_{m=-j}^{j} H_{x,m} x_m \\ &= N\xi_x [\sum_{m=-j+1}^{j} x_m + \sum_{m=-j+2}^{j} x_m + \ldots + \sum_{m=j}^{j} x_m] \\ &\quad + [Z_{x,-j} \sum_{m=-j+1}^{j} x_m + Z_{x,-j+1} \sum_{m=-j+2}^{j} x_m + \ldots \quad + Z_{x,j-1} \sum_{m=j}^{j} x_m] \end{aligned} \tag{50}$$

From Eq. (8), it can be seen that

$$\sum_{m=-j}^{j} H_{x,m} x_m = \sum_{m,n} F_{x,m,n} x_m = 0 \tag{51}$$

Appendix C

Calculation of misalignment error component ξ_y : Similar to $H_{x,m}$, the following equation for $H_{y,m}$ with $j = -\frac{N-1}{2}$ can be constructed, i.e.,

$$\begin{aligned}
&\sum_{m=-j}^{j} H_{y,m}x_m \\
&= H_{y,-j}x_{-j} + \{[H_{y,-j+1} - H_{y,-j}] + H_{y,-j}\}x_{-j+1} + \ldots \\
&\quad + \{[H_{y,j} - H_{y,j-1}] + [H_{y,j-1} - H_{y,j-2}] + \ldots + H_{y,-j}\}x_j \\
&= H_{y,-j}\sum_{m=-j}^{j} x_m + [H_{y,-j+1} - H_{y,-j}]\sum_{m=-j+1}^{j} x_m \\
&\quad + \ldots + [H_{y,j} - H_{y,j-1}]\sum_{m=j}^{j} x_m
\end{aligned} \tag{52}$$

Substituting Eq. (47) into (52), and noting $\sum_m^j = -j_m^x = 0$, one can obtain

$$\begin{aligned}
&\sum_{m=-j}^{j} H_{y,m}x_m \\
&= N\xi_y[\sum_{m=-j+1}^{j} x_m + \sum_{m=-j+2}^{j} x_m + \ldots + \sum_{m=j}^{j} x_m] \\
&\quad + N\xi_\theta[x_{-j}\sum_{m=-j+1}^{j} x_m + x_{-j+1}\sum_{m=-j+2}^{j} x_m + \ldots \quad + x_{j-1}\sum_{m=j}^{j} x_m] \\
&\quad + [Z_{y,-j}\sum_{m=-j+1}^{j} x_m \quad + Z_{y,-j+1}\sum_{m=-j+2}^{j} x_m + \ldots + Z_{y,j-1}\sum_{m=j}^{j} x_m]
\end{aligned} \tag{53}$$

From Eq. (8), it also can be seen that

$$\sum_{m=-j}^{j} H_{y,m}x_m = \sum_{m,n} F_{y,m,n}x_m = 0 \tag{54}$$

As ξ_θ has been calculated out in Appendix A, ξ_y can be figured out by Eqs. (53) and (54).

Author details

Chuxiong Hu[1,2*] and Yu Zhu[1,2]

*Address all correspondence to: cxhu@tsinghua.edu.cn

1 State Key Lab of Tribology, Department of Mechanical Engineering, Tsinghua University, Beijing, China

2 Beijing Key Lab of Precision/Ultra-precision Manufacturing Equipment and Control, Tsinghua University, Beijing, China

http://dx.doi.org/10.5772/62761

References

[1] M. R. Raugh. Auto calibration method suitable for use in electron beam lithography. United States, US Patent. March 7, 1984.

[2] X.-J. Wan, C.-H. Xiong, X.-F. Wang, X.-M. Zhang, and Y.-L. Xiong. A machining-feature-driven approach to locating scheme in multi-axis milling. International Journal of Machine Tools &; Manufacture. 2010, 50 (1): 42–50.

[3] C. Hu, B. Yao, and Q. Wang. Coordinated adaptive robust contouring control of an industrial biaxial precision gantry with cogging force compensations. IEEE Transactions on Industrial Electronics. 2010, 57 (5): 1746–1754.

[4] C. Hu, B. Yao, and Q. Wang. Integrated direct/indirect adaptive robust contouring control of a biaxial gantry with accurate parameter estimations. Automatica. 2010, 46 (4): 701–707.

[5] C. Hu, B. Yao, and Q. Wang. Global task coordinate frame-based contouring control of linear-motor-driven biaxial systems with accurate parameter estimations. IEEE Transactions on Industrial Electronics. 2011, 58 (11): 5195–5205.

[6] C. J. Evans, R. J. Hocken, and W. T. Estler. Self-calibration: reversal, redundancy, error separation, and 'absolute testing. Annals of the CIRP. 1996, 35 (2): 617–632.

[7] J. Kawagoe and T. Kawasaki. A new precision digital phase meter and its simple calibration method. IEEE Transactions on Instrumentation and Measurement. 2010, 59 (2): 396–403.

[8] S.-H. P. Won and F. Golnaraghi. A triaxial accelerometer calibration method using a mathematical model. IEEE Transactions on Instrumentation and Measurement. 2010, 59 (8): 2144–2153.

[9] M. T. Takac, J. Ye, M. R. Raugh, et al. Self-calibration in two dimensions: the experiment. In Proceedings of SPIE Metrology, Inspection, and Process Control for Microlithography, Bellingham, 1996, pp. 130–146.

[10] M. R. Raugh. Two-dimensional stage self-calibration: role of symmetry and invariant sets of points. Journal of Vacuum Science &; Technology B. 1997, 15 (6): 2139–2145.

[11] J. Ye. Errors in high-precision mask making and metrology. Ph.D. Thesis, Stanford University, 1996.

[12] U. Stumper. Uncertainties of VNA S-parameter measurements applying the TAN self-calibration method. IEEE Transactions on Instrumentation and Measurement. 2007, 56 (2): 2047–2052.

[13] T. Barry, G. Fuller, K. Hayatleh, and J. Lidgey. Self-calibrating infrared thermometer for low-temperature measurement. IEEE Transactions on Instrumentation and Measurement. 2011, 60 (6): 2047–2052.

[14] Y. H. Jeong, J. Dong, and P. M. Ferreira. Self-calibration of dual-actuated single-axis nanopositioners. Measurement Science and Technology. 2008, 19 (4): 1–13.

[15] S. Yoo and S. W. Kim. Self-calibration algorithm for testing out-of-plane errors of two-dimensional profiling stages. International Journal of Machine Tools &; Manufacture. 2004, 44: 767–774.

[16] M. Xu, T. Dziomba, G. Dai, and L. Koenders. Self-calibration of scanning probe microscope: mapping the errors of the instrument. Measurement Science and Technology. 2008, 19 (2): 1–6.

[17] Q. C. Dang, S. Yoo, and S.-W. Kim. Complete 3-D self-calibration of coordinate measuring machines. Annals of the CIRP. 2006, 55 (1): 1–4.

[18] M. T. Takac. Self-calibration in one dimension. In Proceedings of SPIE 13th Annual BACUS Symposium on Photomask Technology and Management, 1993, pp. 80–86.

[19] M. R. Raugh. Absolute two-dimensional sub-micron metrology for electron beam lithography: a theory of calibration with applications. Precision Engineering. 1985, 7: 3–13.

[20] J. Ye, M. T. Takac, C. N. Berglund, et al. An exact algorithm for self-calibration of precision metrology stages. Precision Engineering. 1997, 20 (1): 16–32.

[21] X. M. Lu. Real-time self-calibration and geometry error measurement in nm level multi-axis precision machines based on multi X–Y encoder integration. Ph.D. Thesis. University of New Mexico, Albuquerque, 2004.

[22] Y. Zhu, C. Hu, J. Hu, and K. Yang. Accuracy and simplicity oriented self-calibration approach for two-dimensional precision stages. IEEE Transactions on Industrial Electronics. 2013, 60 (6): 2264–2272.

[23] M. Xu, T. Dziomba, G. Dai, and L. Koenders. Self-calibration of scanning probe microscope: mapping the errors of the instrument. Measurement Science and Technology. 2008, 19 (2): 1–6.

[24] C. Hu, Y. Zhu, J. Hu, M. Zhang, and D. Xu. A holistic self-calibration algorithm for X–Y precision metrology systems. IEEE Transactions on Instrumentation and Measurement. 2012, 61 (9): 2492–2500.